Eur. Phys. J. Appl. Phys. (2016) 74: 24608
DOI: 10.1051/epjap/2015150316

THE EUROPEAN PHYSICAL JOURNAL APPLIED PHYSICS

Regular Article

Cold sprayed copper coating: numerical study of particle impact and coating characterization*

Yamina Mebdoua[a], Yazid Fizi, and Nadjet Bouhelal

Centre de Développement des Technologies Avancées, Cité 20 août 1956, BP 17 Baba Hassen, Alger, Algeria

Received: 23 June 2015 / Received in final form: 1 July 2015 / Accepted: 26 November 2015
Published online: 3 May 2016 –

Abstract. Cold spraying technique is a promising process fabricating high quality metallic coatings. This work concerns both numerical and experimental investigations of cold sprayed copper coating taking into account impact conditions including, particle velocities and temperature, gas pressure and material nature. The conducted numerical study is an examination of the deformation behavior of Cu particles sprayed onto steel substrate using Abaqus/explicit software, allowing a good understanding of the deposition characteristics of copper particles and the effect of particle velocity on the coating microstructure. The numerical results show that particle impact velocity has a significant effect on its morphology; Lagrangian method exhibits an excessive distortion of the elements in the case of high impact velocity and fine meshing size, whereas simulation of particle impact using arbitrary Lagrangian-Eulerian (ALE) method is close to the experimental observations.

Nomenclature

A, B, c, m, n	Parameters of Johnson cook constitutive model
ε_{p}	Equivalent plastic strain
$\dot{\varepsilon}_{\mathrm{p}}$	Equivalent plastic deformation rate
T	Temperature
T_{m}	Melting temperature
T_{r}	Reference or transition temperature
ν	Poisson's ratio
P	Total bending force
E_0	Elastic modulus of the bulk material
W	Deflection
$\dot{\epsilon}_0$	Reference strain rate
σ	Yield stress
S_{c}	Coating stiffness
S_{b}	Bending stiffness
S_{t}	Tensile stiffness

1 Introduction

The cold spray process is an emerging deposition process utilizing supersonic gas jet where unmolten and accelerated particles plastically deform upon impact onto the substrate, the deformed particles consolidate with the substrate and their stacking forms the coating [1].

The process allows mainly metallic coatings with high quality coating and low cost compared to those performed with other thermal spraying processes.

In cold spray process, particles whose size is ranging from 1 to 50 μm, are introduced into a supersonic gas flow where they are dragged and accelerated toward the substrate. The supersonic gas flow is generated using a convergent-divergent de Laval type nozzle [1–4]. A cold sprayed coating is build up through a successive layering of plastically deformed particles consolidated with a substrate or with the already deposited particles at a temperature below the melting point of the sprayed material. Cold spraying has been extensively studied thanks to its advantages compared to the conventional thermal spraying techniques. It allows the deposition of a wide range of metals and alloys [4]. In this process, the coating is rigid with an easy controlled thickness, a low porosity rate, and free from oxidation. Moreover, the particles are deposited in their solid state and therefore, the coating keeps the bulk material properties. Bonding mechanism of cold sprayed particles has been extensively studied and still not well understood due to the short duration in which the impact and deformation processes can occur [5–7], and thus, the observation of the entire deformation phenomenon with the existing experimental tools is impossible.

Actually, authors assume that particle deformation may disturb a thin oxides film on the substrate surface inducing a consolidation of the particle with substrate under a high local pressure between the deformed particle and the substrate which provide a consolidation of the particle to the substrate, and bonding can occur. Such a

[a] e-mail: ymebdoua@cdta.dz

* Contribution to the topical issue "Materials for Energy Harvesting, Conversion and Storage (ICOME 2015) - Elected submissions", edited by Jean-Michel Nunzi, Rachid Bennacer and Mohammed El Ganaoui

mechanism is similar to other bonding process occurring in other processes such as shock wave powder compaction [4,8]. The interaction between the impacted particle and the substrate requires a complementary numerical approach to study the bonding mechanism in cold sprayed coating.

Numerous studies used Abaqus and Ls-Dyna to investigate the impact and plastic deformation of micron-sized particles in cold spray process [9–11]. These two finite elements tools were used to solve engineering issues including dynamic processes. In this study, numerical investigation of cold sprayed copper particle impact behavior was conducted making use of Abaqus software. Various combinations of calculations and fundamental phenomena of particle deformation were examined and discussed. This study aims also to examine the microstructure and the mechanical properties of cold sprayed copper coating. The elastic modulus was determined using analytical, numerical and experimental methods. An analytical method developed by Hashin-Hasselman was also used in this investigation to examine the capability of this model to estimate the mechanical behavior of the coating.

2 Numerical modeling

A micron-sized single particle and multi-particle impact behavior were simulated using a finite elements method (FEM). The model predicts the deformation of the impacted particles undergoing high impact velocities, and the coating characteristics. The impact behavior of particles onto substrate was modeled using an explicit FEA Abaqus program. 2D axisymmetric models were used to examine the impact of copper particle of 25 μm of diameter on a steel substrate (SS). The width and height of the substrate were taken to be 500 μm and 100 μm, respectively. The nominal meshing size for the particle was 0.6 μm. In this model, the geometries are partitioned by the four-node bilinear axisymmetric quadrilateral elements with reduced integration and hourglass control (CAX4R). The designed model is a two-dimensional plan strain with multiple particle configurations. A surface-to-surface penalty contact algorithm with a balanced contact pair formulation and a self-contact algorithm were specified for all interface regions with inter-particle friction. All contact surfaces in the model were constrained to remain in contact during the impact process [12].

An empirical model of Johnson-Cook was used in order to predict the dependence of the material temperature on the material deformation. The model includes strain hardening, strain rate hardening and thermal softening effects [13].

The yield stress defined in the model is given as follow:

$$\sigma = (A + B\varepsilon_{\mathrm{p}}^{n})(1 + C\ln(\dot{\varepsilon}^{*}) - (1 - (T^{*}))^{m}), \qquad (1)$$

where A, B, n, C, m are the constants dependent on materials. $\dot{\varepsilon}^{*}$ is the effective plastic strain rate normalized with respect to a reference strain rate $(\dot{\varepsilon}_{\mathrm{p}}/\dot{\varepsilon}_{0})$. T^{*} is a homologous temperature defined as follow [11]:

$$T^{*} = \begin{cases} 0 & \text{for } T < T_{\mathrm{r}} \\ ((T - T_{\mathrm{r}})/(T_{\mathrm{m}} - T_{\mathrm{r}})) & \text{for } T_{\mathrm{r}} \leq T \leq T_{\mathrm{m}} \\ 1 & \text{for } T > T_{\mathrm{r}} \end{cases}. \qquad (2)$$

Table 1. Material properties of the metal used in this simulation [11].

Density ρ (kg m^{-3})	8960
Elastic modulus E (GPa)	124
Poisson's ration ν	0.34
Specific heat C_{p} (J kg^{-1} °C^{-1})	383
Yield strength A (MPa)	90
Hardening coefficient B (MPa)	292
Strain-hardening exponent n	0.31
Strain rate C	0.02
Softening exponent m	1.09
Melting temperature T_{m} °C	1083
Reference temperature T_{r} °C	25
Reference strain rate (s^{-1})	1

The mechanical and thermal properties of the sprayed material were assumed to be isotropic. The properties used in the calculations are presented in Table 1.

The initial particle and substrate temperatures were assumed to be at room temperature. Plastic deformation, in materials, induces temperature rise when plastic deformation energy is dissipated as heat. For most metals, experiments show that the fraction of the plastic deformation converted into heat is of the order of 0.9. This implies that 10% of the total work of deformation goes into material as defects [14]. The particle/substrate interaction was implemented using surface-to-surface contact (explicit) formulation available in Abaqus software.

3 Experimental procedure

Copper is a nonferrous metal, which has a superior energy absorption coefficient, photoelectric conversion efficiency of absorption, electric and thermal conductivities. These properties make it a good candidate material in energy applications; it has also, an excellent cold sprayability that is why, it has been widely studied experimentally. In this study, the elastic modulus of the coating was experimentally determined using nano-indentation tensile test and three-point bending test. In addition, the elastic modulus was calculated using analytical method.

Instrumented nano-indentation measurements were also performed on the coating cross-sections of the three examined samples in order to obtain experimental load-displacement curves of the Cu coating. These measurements were performed using nano-indenter with a Birkovich tip of CSM equipment, which resolutions were 0.04 μN in force and 0.04 nm in displacement. The experiment involved a controlled displacement with an indentation velocity of 0.04 μm/s. When the maximum available depth was reached, the indenter was held for 10 s, and then

Fig. 1. Three point bending test set-up.

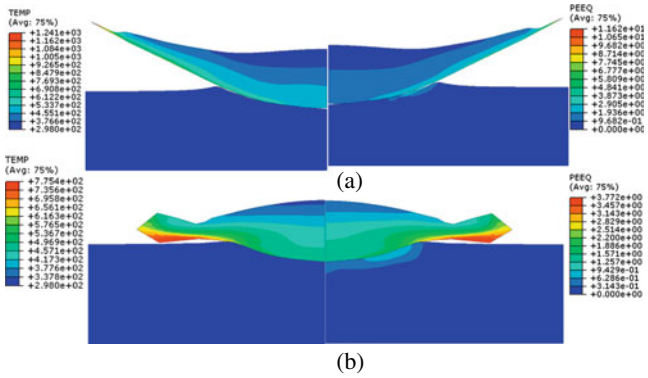

Fig. 2. Simulated contours of PEEQ and temperature using the Lagrangian (a) and ALE (b) methods.

moved back with the same velocity. A Birkovich indenter with a maximum load of 300 mN was used. The maximum indentation depth from different tests was 2.497 μm.

Tensile specimens were made from cold sprayed Cu coating deposited on steel substrate. The coating was separated from the substrate and machined to coincide with ASTME8M-04 [15]. Due to limitations of coating thickness the samples were cut parallel to splat plane also known as the transverse direction. Tensile tests were performed using a screw driven testing machine (Zwick/Roell Z.100) at a strain rate of 10^{-4} s^{-1} until specimens fracture. Three-point bend tests (Fig. 1) were performed using a screw driven testing machine at a rate of 0.12 mm/min, separation of the coating was not required. The subsized bend samples were cut to 20 mm × 85 mm × 5 mm. The bending tests were performed using five specimens at room temperature in accordance to ASTM E290-09 standard [15]. The bending stiffness (S_b) and tensile stiffness (S_t) are defined by the equations (3) and (4) from which the modulus of the coating can be calculated [16,17].

$$S_\mathrm{b} = \frac{1}{3}\left[E_\mathrm{c}^* h_\mathrm{c}^* + E_\mathrm{s}^*(h_\mathrm{t}^3 - h_\mathrm{c}^3)\right] - S_\mathrm{t}\delta^2, \tag{3}$$

$$S_\mathrm{t} = E_\mathrm{c}^* h_\mathrm{c} + E_\mathrm{s}^* h_\mathrm{s}, \tag{4}$$

where

$$\delta = \frac{1}{2S_\mathrm{t}}\left[E_\mathrm{c}^* h_\mathrm{c}^2 + E_\mathrm{s}^*(h_\mathrm{t}^2 - h_\mathrm{c}^2)\right], \tag{5}$$

and

$$E_\mathrm{s}^* = \frac{E_\mathrm{s}}{1-\nu_\mathrm{s}^2}; \quad E_\mathrm{c}^* = \frac{E_\mathrm{c}^*}{1-\nu_\mathrm{c}^2}. \tag{6}$$

The subscripts c, s and t denote the coating, substrate, and total, respectively. The thickness of the coating and the substrate are denoted by h.

In the case of the three-point bend test of a single uniform material, the bending stiffness (S_b) can be calculated as follow:

$$S_\mathrm{b} = PL^3/48W, \tag{7}$$

where L is the span between pins as shown in Figure 1. Therefore, by solving equations (3) through (7), the elastic modulus of the coating E_c can be calculated.

4 Results of numerical modelling

4.1 Deformation behavior of sprayed particles

Figure 2 shows the contours of effective plastic strain (PEEQ) after a single copper particle impact on the already deposited copper coating on steel substrate. Calculations were performed using the Lagrangian and arbitrary Lagrangian-Eulerian (ALE) method at the velocity of 650 m/s.

The calculations using these two methods presented in Figure 2, show different shapes of the deformed particles and substrate. Lagrangian method allows observation of temperature localization at the interface. A maximum PEEQ at the interface is obtained using the Lagrangian method.

4.2 Effect of impact velocity

Figure 3 shows the time evolution of the equivalent plastic strain on the surface of a copper particle for different values of impact velocity. The particle impact velocities used in the calculations are 300, 500, 700 and 900 m/s.

Figure 3a, shows a rapid increase of the plastic strain with an average rate up to 2.4×10^9 s^{-1}, before reaching its final value of about 3, 5, 10 corresponding to the velocity values of 300, 500 and 700 m/s respectively. Whereas the plastic strain determined with impact velocities of 900 m/s shows a decrease in the equivalent plastic strain. This behavior is attributed to the presence of high strain gradients in the interface particle/substrate. In the case of ALE model, Figure 3b shows a decrease in the equivalent plastic strain with the time. This behavior could be explained by errors due to adaptive meshing algorithm in the remapping phase. It is well known that the Lagrangian description may be distorted, especially with the large deformation speeds reached in cold spray process. Therefore, the morphologies of the deformed particles become inaccurate and may not represent actual deformations. Figure 4a presents the contour of the Von-mises stress with the impact velocity of 1100 m/s. The program is terminated at 9 ns after impact. Figure 4b presents the

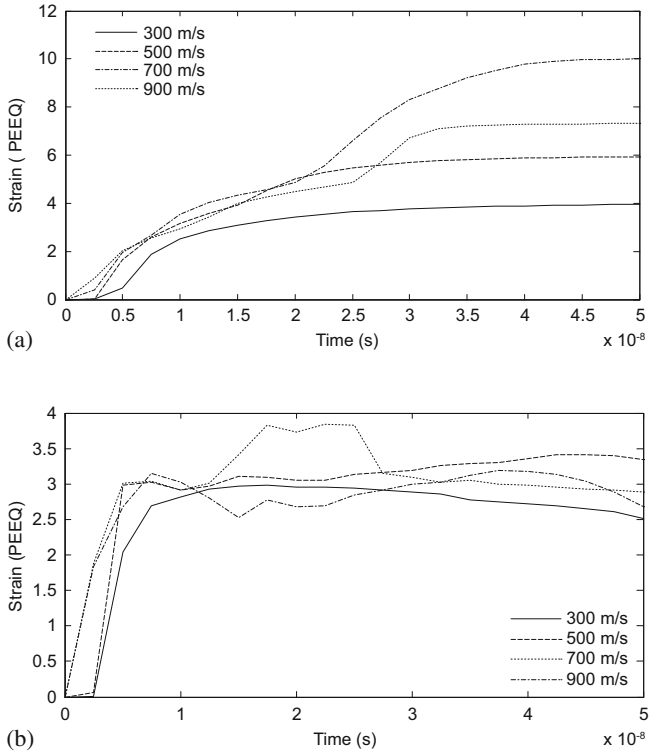

Fig. 3. Time evolution of effective plastic strain of copper particle under different particle velocities using Lagrangian (a) and ALE method (b).

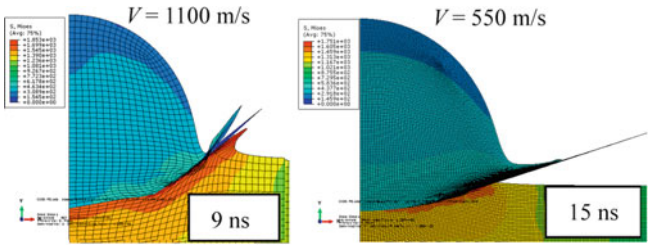

Fig. 4. Contours of Von-mises stress at the contact interface for the particle with the meshing size of 0.6 (a) and 0.1 μm (b) modeled by Lagrangian method.

contour of the Von-mises at the interfacial region of one particle with a meshing size of 0.1 lm using Lagrangian method. The distortion of the Lagrangian grid results in the abnormal termination of the program at 15 ns after impact.

Numerical analysis [18] obtained independently of the meshing size shows better deformation morphologies than that obtained by the Lagrangian approach. Figure 5 shows the impact of a particle with initial temperature of 673 K, and an impact velocity of 550 m/s, in this case a good consistency was obtained between the deformed particle morphology observed by SEM and calculated by ALE method.

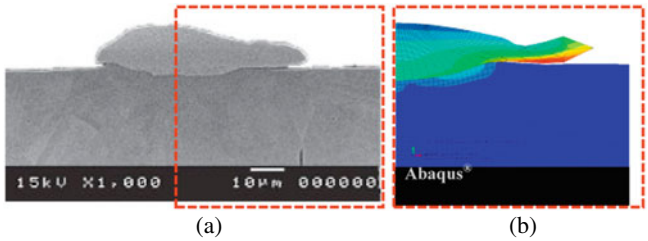

Fig. 5. Experimental [19] (a) and simulated morphologies of splats sprayed on SS substrate at 673 K.

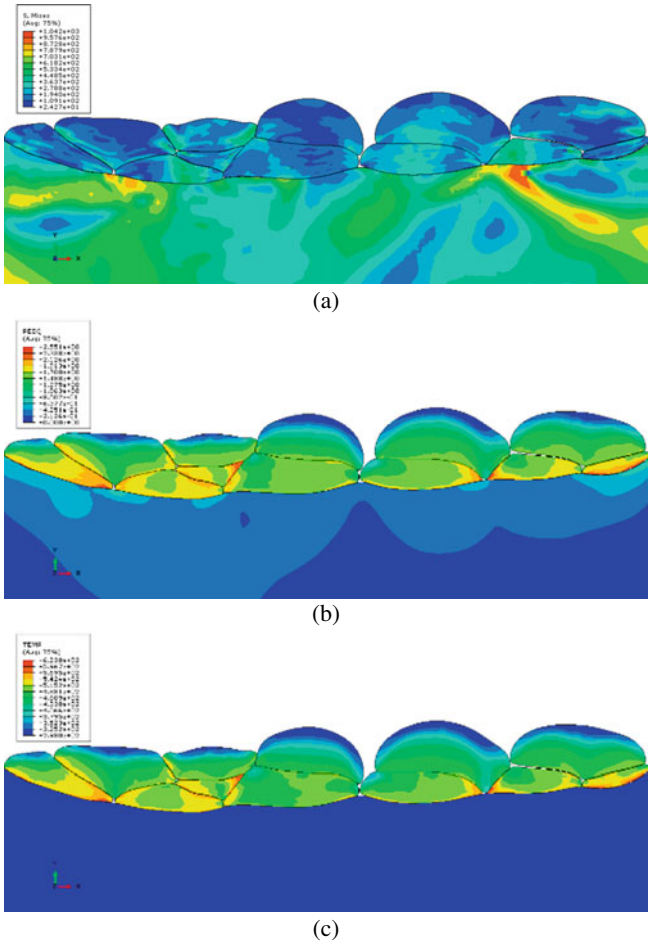

Fig. 6. Contours of the Von-mises stress (a), effective plastic strain (b) and temperature (c) of multi-particle impacting on the SS substrate at 250 ns modeled by ALE method.

4.3 Multi-particle impact process

The simulation of multi-particles impact process is of great importance to better understand the bonding mechanism and the cold sprayed coating properties. ALE method is used to simulate the multi-particle impact process. The sprayed copper particles size used in these calculations are: 25, 35, 40, 45 and 50 μm, and impact velocity values ranging from 450 to 650 m/s. The particles and the substrate were kept at the same initial temperature (298 K). Figure 6 shows contours of Von-mises stress, effective

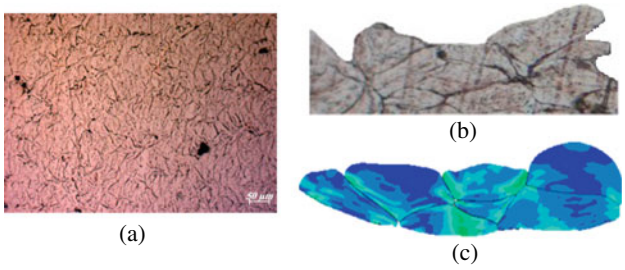

Fig. 7. SEM Micrograph of cold sprayed copper coating cross-section, (a) experimental, (b) calculated, (c) morphologies of particle deformed.

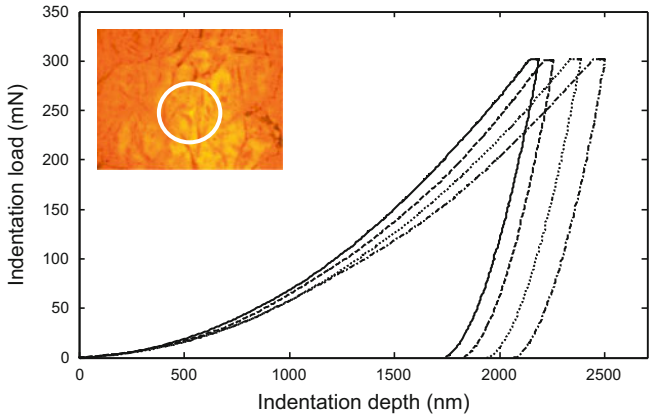

Fig. 8. Load-displacement curves of cold sprayed copper coating.

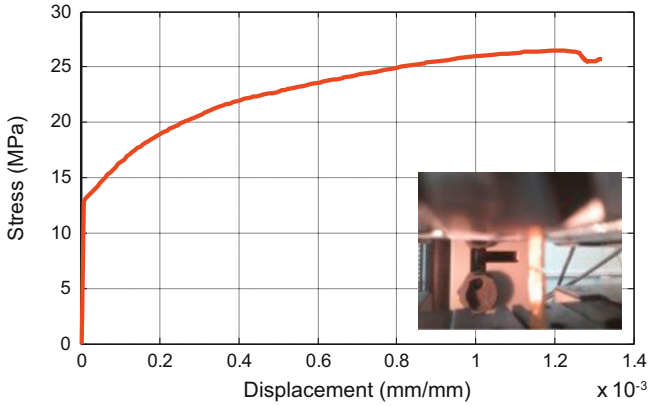

Fig. 9. A typical stress-strain curve obtained from copper coating tensile test. The inset is the fractured sample after tensile test.

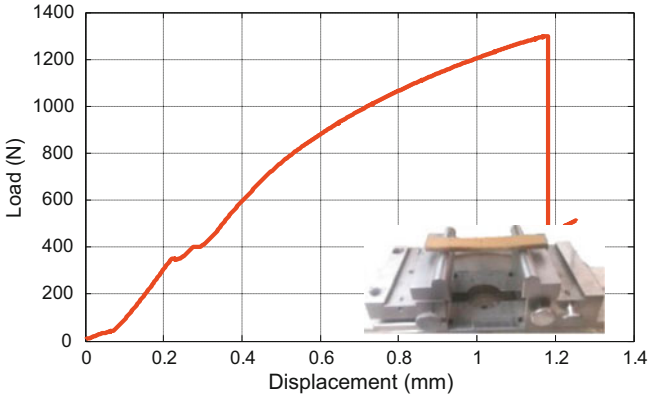

Fig. 10. Loading curve resulting from bending test, the inset is the fractured sample after bending test.

plastic strain and temperature of multi-particle impacting on the substrate.

We can see in Figure 6b, packed particles with irregular shapes due to impact and deposition of the subsequent sprayed particles. The later deposited particles are not well flattened or well deformed; they have the same shape as that observed in the case of a single particle. A high plastic strain is observed between the first deposited particles and the substrate, and between neighboring particles inside the coating. This situation may indicate the bonding of the coating.

5 Experimental results

Figure 7 shows a cross-section of copper coating. The deformed particles are well stacked on each other and well bonded to the substrate, with a very low porosity in the whole coating. The deformed particles have elongated morphologies.

In this study, Hashin-Hasselman [19,20] equation was used to calculate the elastic modulus. This is the most commonly applied model estimating the material modulus taking into account porosity. The elastic modulus is obtained from SEM image, which is taken from different positions along the polished cross-section of the coating.

The Hashin-Hasselman equation is defined as follow:

$$E^* = E_0 \left[1 + \frac{A'p}{1-(A'+1)\,p}\right], \tag{8}$$

where A' is a constant equal to -33.4, p is the volume fraction of all voids, cracks, and interfaces between splats. By substituting the above values in Hashin-Hasselman equation, the estimated elastic modulus of the coating (E^*) was of the order of 92.72 GPa.

The depth-sensing indentation measurement was used to determine the hardness and the Young's modulus. Figure 8 shows the load-displacement curves of the copper coating. The average modulus of elasticity of the coating is about 114.10 ± 8.4 GPa and the average hardness was 3.06 ± 0.40 GPa.

The tensile test samples in transverse direction were difficult to obtain due to sub-sized samples and the thin brittle coating structure requiring special machining. Transverse tensile specimens were achieved with much difficulty, it was nearly impossible to fabricate specimens in the longitudinal direction because the required coating thickness to machine a cross section into a standard dog-bone shape would have to be unreasonably thick.

Therefore, we did not conduct an experiment in longitudinal direction of the tensile test characterization [21]. A typical stress-strain curve measured from the tensile test on cold sprayed copper coating is shown in Figure 9. The average elastic modulus is about 8.93 ± 0.40 GPa for three tensile test samples.

The three-point bend test was completed on the samples from which the elastic modulus of the coating is of the order of 40.61 ± 1.50 GPa. The bend test provides the modulus in the longitudinal direction. A standard loading (load-displacement) diagram is shown in Figure 10 for the three-point bend test.

6 Conclusion

Divers methods were used in this work to identify the elastic modulus of cold sprayed copper coating. The tensile test modulus was significantly lower than that obtained by indentation and three bend tests. This could be due to the small sample sizes and the presence of voids. The impact of copper particles in cold spraying method has been numerically investigated using both methods: Lagrangian and ALE. The numerical result show that the impact velocity has a significant effect on the particle deformation (particle morphologies). It has been shown that lagrangian method exhibits an excessive distortion of the elements in the case of simulation with high impact velocity and fine meshing size. Simulation of particle impact using ALE method is close to the experimental observation.

In a future work, the effect of surface roughness and 3D modeling will be necessary to take into account more real conditions of particle impact.

References

1. P.L. Fauchais, J.V. Heberlain, M.I. Boulos, *Thermal Spray Fundamentals: From Powder to Part* (Springer Science + Business Media, New York, 2014)
2. S.V. Klinkov, V.F. Kosarev, M. Rein, Aerosp. Sci. Technol. **9**, 582 (2005)
3. A. Papyrin, Adv. Mater. Process. **159**, 49 (2001)
4. T. Shmidt, F. Gartner, H. Assadi, H. Kreye, Acta Mater. **54**, 729 (2006)
5. W.-Y. Li, C.-J. Li, Y.-Y. Wang, G.-J. Yang, Acta Metall. Sin. **41**, 282 (2005)
6. T. Schmidt, F. Gartner, T. Stoltenhoff, H. Kreye, H. Assadi, in *Proceeding of International Thermal Spray Conference ITSC 2005, Basel, Switzerland*, edited by E.F. Lugscheider (DVS-Verlag, Düsseldorf, 2005), p. 232
7. T.H. Van Steenkiste, J.R. Smith, R.E. Teets, Surf. Coat. Technol. **154**, 237 (2002)
8. R.C. Dykhuizen, M.F. Smith, D.L. Gilmore, R.A. Neiser, X. Jiang, S. Sampath, J. Therm. Spray Technol. **8**, 559 (1999)
9. H. Assadi, F. Gartner, T. Stoltenhoff, H. Kreye, Acta Mater. **51**, 4379 (2003)
10. C.J. Li, W.Y. Li, H.L. Liao, J. Therm. Spray Technol. **15**, 212 (2006)
11. W.Y. Li, H.L. Liao, C.J. Li, H.-S. Bang, C. Coddet, Appl. Surf. Sci. **253**, 5084 (2007)
12. G.R. Johnson, W.H. Cook, Eng. Fract. Mech. **21**, 31 (1985)
13. A. Meyers, A. Marc, *Dynamic Behavior of Materials* (Wiley, New York, 1994)
14. ASTM International, *Annual Book of ASTM Standards*, vol. 03.01, 1997
15. ASTM, Standard test methods for bend testing of material for ductility, in *ASTM E290- 9. ASTM International, West Conshohocken, PA, 2009*
16. J.H. You, T. Hoschen, S. Lindig, J. Nucl. Mater. **348**, 94 (2006)
17. J. Mencík, *Mechanics of Components with Treated or Coated Surfaces. Solid Mechanics and its Applications*, edited by G.M.L. Gladwell, vol. 42 (Kluwer Academic Publisher, Dordrecht, Netherlands, 1995), p. 366
18. S. Yin, G. Wang, B.P. Xu, W.Y. Li, J. Therm. Spray Technol. **19**, 1032 (2010)
19. Z. Hashin, J. Appl. Mech.-T. ASME **29**, 143 (1962)
20. D.P. Hasselman, J. Am. Ceram. Soc. **45**, 452 (1962)
21. C. Leither, J. Risan, M. Bashirzadeh, F. Azarmi, Surf. Coat. Technol. **235**, 611 (2013)